Reversible Switch Memory Effect in Hydrogen-Terminated Ultrananocrystalline Diamond

Moshe Tordjman, Asaf Bolker, Cecile Saguy, Emanuel Baskin, Paola Bruno, Dieter M. Gruen, and Rafi Kalish**

Innovative memory switch devices require reliable bistable conductance properties. It would be desirable if such bistable characteristics were available in robust solid state materials, such as diamond, which benefit from outstanding physical properties. A bistable current with reversible switching effect from surface transfer doped ultrananocrystalline diamond thin films measured by electron field emission is reported. This switching is manifested by the appearance of huge jumps in the current emission, up to four orders of magnitude, that occur at specific extracting electric field values. Persistent hysteresis is exhibited whenever the field is ramped down. It is proposed that these phenomena are the result of resonant-tunneling through a double barrier junction composed of tetrahedral amorphous carbon (ta-C)/nanodiamond/adsorbent/vacuum. This finding may pave the way for the realization of novel types of memory switch devices with unprecedented performance.

1. Introduction

Nanoscale memory-switch circuits may play a crucial role in novel logic, memory, and processing devices, determining the basic efficiency of these devices. The realization of nanoscale memory-switch circuits has been attempted on various types of materials employing nonlinear resistance effects or quantum electronic transport phenomena.[1] One of the promising memory effects has been demonstrated in organic materials,[2,3] showing viable bistable switching characteristics. High-speed switching has been ameliorated in solid-state heterostructures, exploiting double-barrier resonant tunneling principles in hybrid composites of amorphous carbon.[4] Although vacuum-based devices benefit from the highest electron velocity ($\approx 3 \times 10^8$ m s^{-1}), yielding high-power and high-frequency devices for microwave amplifiers,[5] they suffer from a lack of reliable bistable characteristics, low on/off ratios, and inconsistent memory windows. Taking into account that two-terminal devices based on graphitic compounds are becoming more significant in electronics architectures,[6] an electron field emission (FE) process on carbon-based nanostructures is expected to offer superior memory-switching devices once reliable bistability behavior can be achieved.

FE from quantum assemblies have been theoretically predicted and experimentally shown to have exceptional properties[7–11] due to sequential tunneling along confined structures in which resonance tunneling plays a major role. Indeed, various configurations showing anomalies in the current–voltage (I–V) curves, such as regions with negative differential conductance[7,12] and steps in the I–V characteristics,[13,14] have been observed. Some years earlier FE resonant tunneling had been investigated in metal samples containing adsorbates on surfaces.[15–17] Recently, resonant behavior has been reported from multiwalled carbon nanotubes covered by chemisorbed molecules (carboxylic moiety or adsorbed water) exhibiting some weak step-like properties in the field emission.[18] These weak step-like properties have been attributed to resonant tunneling through quantum states formed by the presence of the adsorbate layer. An abrupt switch-on of one order of magnitude, step-like feature has also been reported by Madaleno et al.[19] for non-hydrogenated nanocrystalline diamond microtip arrays. However no hysteresis and no repeatability or reversibility has been shown.

In the present work we report the observation of a reversible hysteretic switching in the FE process in ultrananocrystalline diamond (UNCD) thin films[20] following surface hydrogenation and exposure to humid air. As a unique property of the diamond surface, this surface treatment is responsible for high p-type surface conductivity, as explained by the electrochemical transfer doping model,[21–23] and is essential for obtaining the results described below.

The FE measurements exhibit consistent electrical bistability with a significant memory window and an on/off ratio of up to 10 000:1 in the emitted current density. An extremely sharp switch-on of the electron emission current is found. It increases abruptly by three orders of magnitude, followed by further successive jumps, each accompanied by plateaus. When the field is ramped down, the FE current remains "on" even at values of

M. Tordjman, A. Bolker, Dr. C. Saguy, Dr. E. Baskin, Prof. R. Kalish
Russell Berrie Nanotechnology Institute
Physics Department and Solid State Institute
Technion–Israel Institute of Technology
Technion City, 32000 Haifa, Israel
E-mail: moise@tx.technion.ac.il; kalish@tx.technion.ac.il
Dr. P. Bruno, Prof. D. M. Gruen
Materials Science Division
Argonne National Lab, Argonne
60439 IL, USA

DOI: 10.1002/adfm.201102193

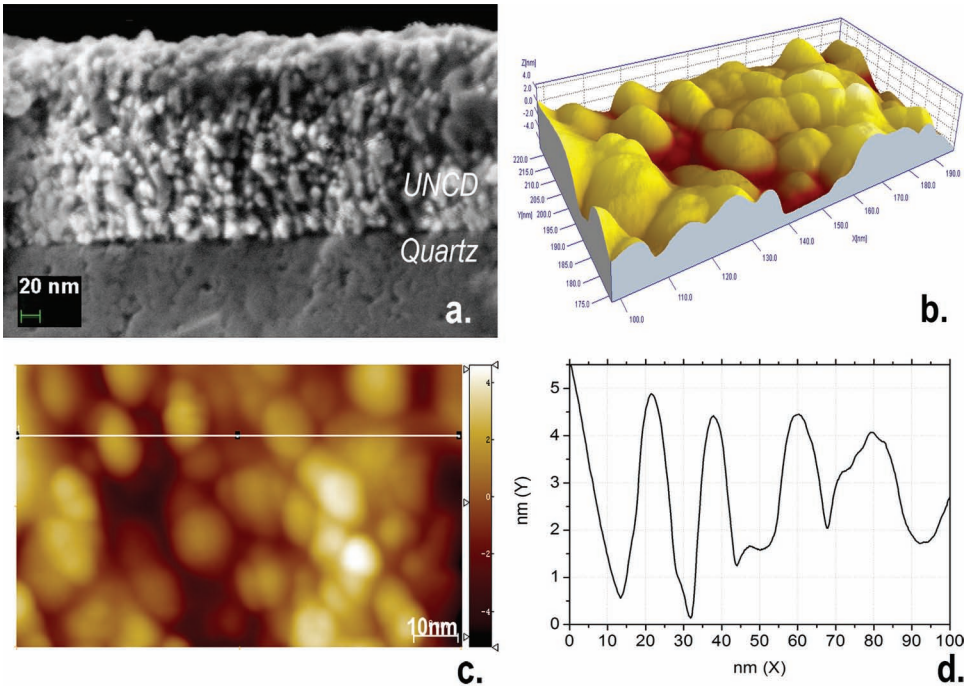

Figure 1. View of a UNCD layer: a) cross sectional high-resolution SEM image of the UNCD layer grown on quartz; b) 3D AFM topography image of the UNCD; c) 2D contact AFM of the UNCD plane view, and d) the corresponding profile of typical diamond grain sizes (5–15 nm).

the field lower than the initial switch-on values. The FE current turns off abruptly, only at substantially lower fields, showing a pronounced hysteresis (memory) effect. These FE data are repeatable, reversible and are observed consistently from the same emission spot and from other spots on the sample for several hundreds of consecutive cycles (>700) during a continuous operation period of ≈20 h. The phenomenon was found to disappear following in situ heating (300 °C) of the UNCD thin film.

2. Results and Discussion

2.1. Surface Characterization

The samples used were UNCD films (300 nm thick) grown on quartz, microwave plasma hydrogenated (H) and exposed to humid air. A cross-sectional high-resolution scanned electron microscopy (SEM) image of a sample is shown in **Figure 1**a. Clear diamond nanograins ranging in size from 5 to 15 nm can be observed (bright regions), separated by amorphous carbon (a-C) nano-"pockets", with typical widths ranging between 1.5 and 2 nm (dark regions in Figure 1a). Atomic force microscopy (AFM) measurements, which also revealed a surface roughness of 3.5 nm and a high density of nanodiamond (ND) grains, are consistent with the SEM results. A 3D AFM image of the UNCD topography is displayed in Figure 1b; a 2D AFM image and its corresponding profile are shown in Figure 1c,d. Based on X-ray photoelectron spectroscopy (XPS) measurements, the amorphous carbon (a-C) surrounding the nanodiamonds was estimated to contain about 85% sp^3 bonded C, i.e., the nanodiamond (ND) grains are separated by tetrahedral amorphous carbon (ta-C). A similar conclusion was obtained from previous results of electrical transport measurements done on the same UNCD material.[24]

2.2. Electrical Observations

The results of repetitive FE measurements on an UNCD sample following surface treatments, such as cleaning in acids, hydrogen plasma treatment, and exposure to humid air, are plotted in **Figure 2** as the log of the current density (J) versus applied electric field (E). The blue lines show the results of consecutive cycles of the current density, $J(E)$, measured with the voltage being sequentially ramped up and down. These curves exhibit successive plateaus separated by abrupt jumps. A persistent hysteresis is measured whenever the voltage is ramped down. Similar results were obtained on different samples from the same UNCD wafer, illustrating the reproducibility and reversibility of the results. One virgin sample was subjected to several cycles of repeated heating and H removal followed by new hydrogenation and exposure to humidity. The results of the FE measurements performed on the same sample after each surface treatment sequence (as described above) for many fields

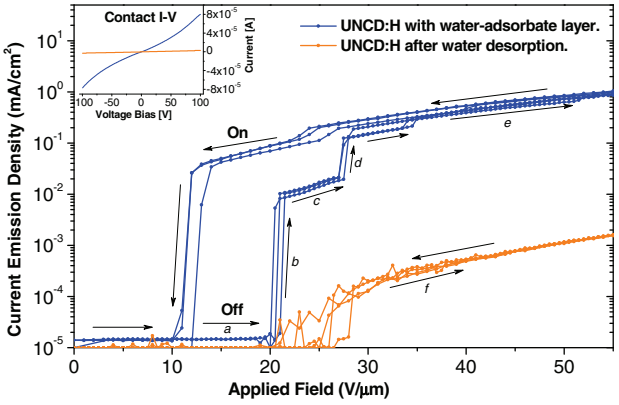

Figure 2. Results of current FE measurements from UNCD layer. The blue lines show consecutive FE cycles from hydrogenated and humid air exposed UNCD layer. The orange lines show consecutive FE cycles from the same sample after in situ heating to 300 °C. Inset: I–V surface contact measurement of the UNCD:H:H_2O before (blue line) and after (orange line) in situ heating. The different stages of the FE marked as a, b, c, d, e, f are discussed in Figure 5.

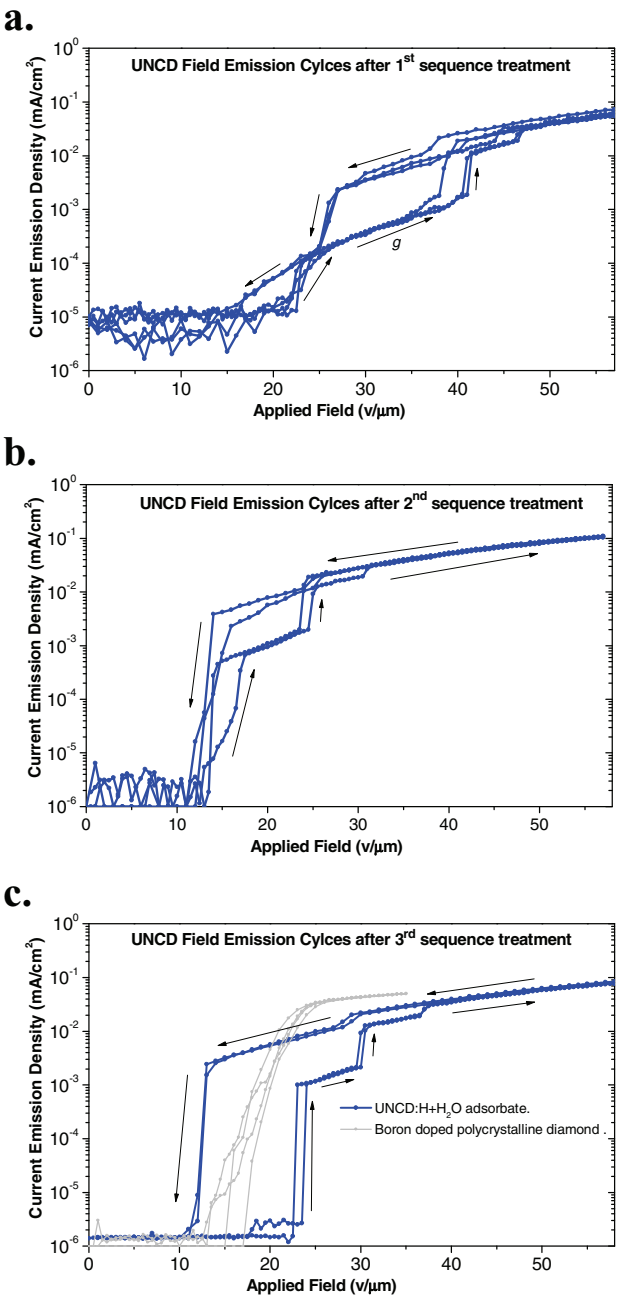

Figure 3. Progressive improvement of the switch-memory properties of the FE from UNCD layer following surface treatment sequences. a) FE cycles of a virgin UNCD sample following a single surface treatment. b) FE cycles of the same sample after a second successive treatment. c) FE cycles after a third successive treatment. Gray lines show typical FE cycles from a boron-doped polycrystalline diamond under the same conditions for comparison.

up/down cycles are shown in **Figure 3**. Figure 3a shows the results for a single treatment on a virgin sample, while Figure 3b,c display, respectively, the results following a second and third successive treatment of the same sample. It should be noticed that the electrical switching properties of the sample progressively improved.

In a different experiment the sample was heated, in situ, to 300 °C, to remove the water thin layer adsorbate from the UNCD:H surface. FE measurements were repeated after letting the sample cool back down to room temperature into vacuum. The result (Figure 2 orange line) shows a very poor (if any) gradual electron emission while ramping the field up and down. *I–V* surface contact measurements of the UNCD:H:H_2O sample were performed at room temperature before and after heating (inset Figure 2). Before heating an almost linear behavior was observed and neither peculiar jumps nor hysteresis effects could be noticed in the *I–V* cycles. This result suggests that the abrupt jumps and hysteretic FE were not caused by irregularities in the electrical conductivity; they must be related to the electron escape process. After heating, the surface conductivity had vanished, and the sample was highly insulating.

2.3. Peculiarities

The present results are in stark contrast with usual Fowler–Nordheim (FN) electron field emission behavior, which is characterized after turn on by a rather gradual rise in the FE current. As a test case, FE from a boron-doped hydrogen terminated polycrystalline diamond sample was measured under the same experimental conditions and indeed showed typical FN field emission properties (Figure 3c gray lines).

The following peculiar results should be noted and require explanation:

1) The FE from the moisture exposed UNCD:H samples switched-on extremely abruptly and exhibited several consecutive jumps.
2) Between the jumps, plateaus in the *J*(*E*) curves with only moderate increases in the emission current were observed.
3) Decreasing the applied field resulted in a completely different behavior: the high emission current was maintained for values of the field substantially lower than those of the ramp-up case (hysteretic behavior). The emission current was characterized by a small and moderated decrease of the current *J*(*E*) until an abrupt turn-off occurred, at a remarkably smaller applied field value (12 V μm^{-1}) than that of the initial turn on field (22 V μm^{-1}) (Figure 2). This was observable for all *J*(*E*) cycles (hysteresis behavior).
4) Heating the sample to 300 °C extinguished all of the above phenomena (Figure 2, orange lines).
5) A repeated surface cleaning followed by microwave hydrogen plasma treatment and exposure to humidity restored, and even sharpened, the switching effect in the FE (Figure 3).

In summary, the resulting FE properties from the hydrogenated humidity-exposed UNCD thin film show a room-temperature reversible hysteretic switching, which exhibits a consistent electrical bistability with endurance of $\approx 10^3$ cycles, a memory window of 9 ± 1 V μm^{-1}, on/off ratio of 10^4 in the emitted current density, and a switch speed expected to be less than 10^{-14} s due to vacuum propagation. In comparison, nanowires metal oxide based materials,[1,2] which are considered as a leading memory technology, show a typical on/off ratio up to 10^4,

switching speed[25] of ≈50 ns, and endurance[26] of more than 10^2 cycles. Molecular[27] and chalcogenide[28] elements show on/off ratios under 10^3, thus placing UNCD as a material of choice among them.

To offer a possible explanation for these peculiar observations one should recall that electron emission from solids depends on the properties of the emission sites and on the availability of electrons at these sites. These are affected in the present case of FE from UNCD by the complex structure of the sample, which is composed of nanocrystalline diamonds embedded in amorphous carbon, and by the unique electrical properties of the outermost diamond nanocrystallites surface, which is H terminated and covered by a thin layer of adsorbed water.

The presently used UNCD samples, when non-hydrogenated, had resistances greater than 10^7 Ω □$^{-1}$. Upon hydrogenation and exposure to humidity, the resistances dropped to 10^4 Ω □$^{-1}$ with Hall-effect sheet hole concentrations of about 9×10^{11} cm^{-2} due to surface transfer doping. This is known in single crystal diamond to result in a surface upwards band bending extending to a depth of several nanometers (8–10 nm). Because the small dimensions of the ND crystallites (5–15 nm) are comparable to the thickness of the band bending, one can assume that the entire volume of the nanocrystallites "turned" p-type. The fact that the observed FE phenomena disappeared after in situ heating at 300 °C, a temperature at which the adsorbed water molecules is known to evaporate from the surface of the diamond,[29] proved the crucial role that the adsorbed water layer had on the measured phenomena. The importance of this layer has also been demonstrated for the case of single-crystal diamond surfaces.[30]

2.4. Electrical Transport

Below we separately discuss the various factors affecting the FE:

1) The emission site. Two different possible emission sites from which electrons can escape to vacuum must be considered: i) from H-terminated water-layer covered diamond nanocrystallites and ii) from amorphous carbon separating the diamond grains or from thin ta-C layers possibly partially covering the diamond nanograins at the surface. Site (i) has a negative electron affinity of $\chi = -1.3$ eV and has undergone a local surface transfer doping that has induced a p-type surface conductivity. As for emission site (ii), electrons have to overcome a potential vacuum barrier[31] of ≈3eV. Hence, emission from site (ii) is expected to increase monotonically with the extracting field.[32]

In the present case the surface of the sample was successively modified by consecutive surface cleanings, followed by exposure to a H plasma. Such treatment is known to etch a-C layers[33] and this has been verified by electron energy loss spectroscopy and XPS measurements. The FE of the sample following repetitive H plasma treatments was found to sharpen (Figure 3), presumably as a result of ta-C removal from the UNCD surface, indicating the importance of the surface state of the outermost ND grains.

2) The availability of electrons at the emission sites. This is complicated by the composite nature of the UNCD sample. The supply of electrons can, in principle, be via a surface path or via the subsurface regions. The pathway along the surface is due to the p-type surface conduction of the ND composed of conductive channels intercepted by the relatively insulating narrow amorphous carbon (ta-C) regions. The pathway below the surface is via ta-C thin regions separated by sections of intrinsic (non-transfer doped) nanocrystallites diamonds. In this pathway, intrinsic nanocrystallites diamonds play the role of insulators and the ta-C pockets are the more conductive part of the composite bulk.

2.5. Emission Mechanism

The fact that the peculiar UNCD's FE phenomenon were shown to be enhanced following each etching plasma treatment allows us to relate the emission mechanism as mostly originating from H-terminated water-layer covered diamond nanocrystallite sites. As noted above, the sample is composed of ND grains separated by ta-C interlayers. In order to depict the emission mechanism from the low-dimensional sites residing in a complex structure, we used a simplified representation based on a 1D periodic heterostructure perpendicular to the surface (**Figure 4**). In this model the two last heterojunctions, behind the surface, are represented by a double barrier tunneling junction composed of ta-C/ND/adsorbent/vacuum. An energy band offset of ≈2.5 eV is obtained between the conducting band minima of the internal diamond grain (with a bandgap energy of E_g= 5.47 eV and χ = 0.5 eV) and ta-C pocket conducting states (with E_g = 2.5 eV and χ = 3 eV[31]). The simplified subsurface structure is described by a finite rectangular quantum well (QW) formed by the ta-C layer surrounded by two asymmetrical potential barriers, the left one being formed by the insulating diamond grain and the right one being that of hydrogenated and humid-air-exposed diamond grain. The typical width of the ta-C layer separating the ND grains, d, ranging from 1.5 nm to 2 nm (as deduced from characterizations), is taken as the QW width range. Although the ND grains vary in size from 5 to 15 nm, the optimal shortest tunneling distance separating two ta-C regions are of the order of ≈1 nm. This is taken as the width of potential barriers through which electrons will preferentially tunnel from one ta-C pocket to another (Figure 4). The spectrum range of the energy levels values, E_n, for the ta-C finite QW can be calculated from the Schrodinger's equation solution for a finite potential well[34] with a varying width, d. This approach can be approximated to the solution for the energy levels of an infinite quantum well case since the differences found in numerical results between the two solutions of this case is small and negligible in comparison to the ranges for each energy level value. The possible energy level range, ΔE_n, is given by the equation:

$$\Delta E_n = (\pi\hbar)^2 n^2 / 2m^* (d)^2 \quad (1)$$

Where QW thicknesses d = 1.5–2 nm, n = 1, 2, and 3 representing the n^{th} energy level, the effective electron mass in ta-C is taken to be of $m^* = 0.87m_e$[35] and is the reduced Planck constant. This leads to three different sub-bands with energies ranging between 0.12–0.21eV, 0.47–0.83 eV, and 1.05–2.5 eV corresponding to the first, second, and third broadened energy

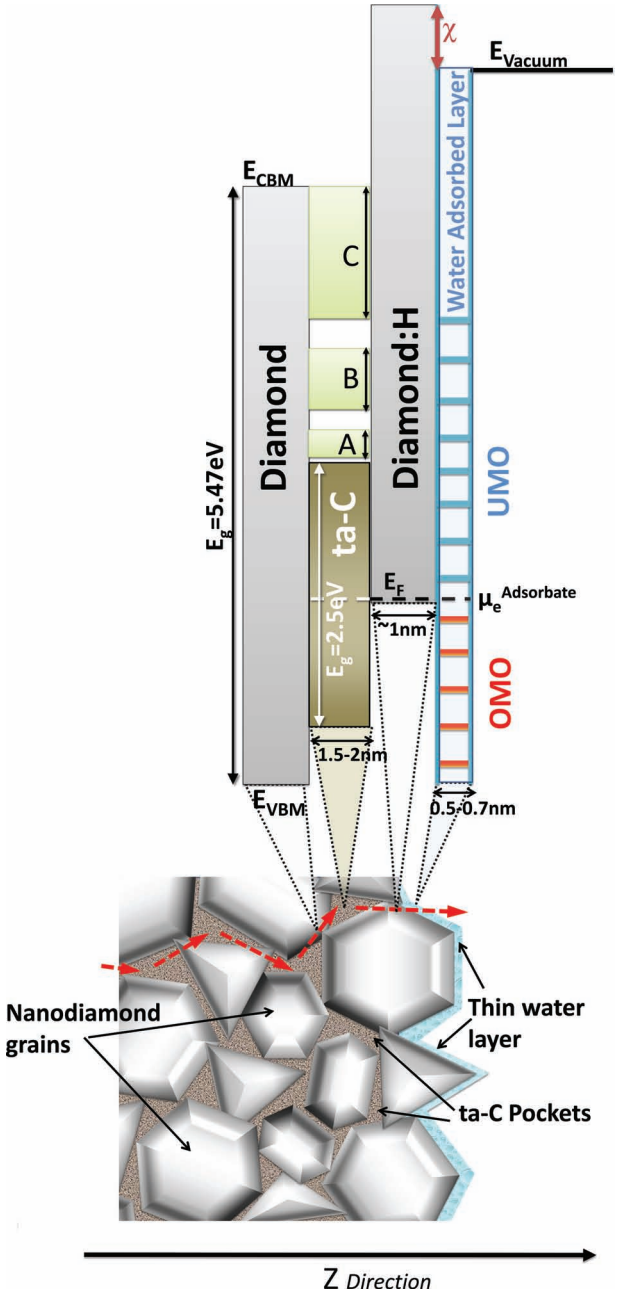

Figure 4. Schematic band diagram of the ND grains and ta-C pockets periodic heterostructure, perpendicular to the surface, in correspondence with the structural UNCD:H:H_2O layer. The outermost transfer-doped ND grain (E_g = 5.47 eV), which has p-type properties and negative electron affinity (χ = –1.3 eV), is covered by a thin water adsorbate layer represented by a QW before the vacuum barrier. The ta-C layer (E_g = 2.5 eV) behind forms a QW between the insulating ND grain (from the bulk) and the outermost ND grain. A, B, and C represent the broadened energy levels in the ta-C QW. The red arrows in the structural UNCD layer sketch represent a typical electron pathway to the emission site.

levels in the representative QW. In this picture the field penetration inside the ta-C QW during the band bending, estimated to be less than 0.04 eV, has been disregarded.

The energy band diagram of the heterostructure in the outermost layer determines the emission properties. The last ta-C QW has asymmetrical potential barriers, where the inner potential barrier is that of the intrinsic ND grain in the bulk and the outer barrier is that of the hydrogenated and adsorbate-covered ND grain facing the vacuum (with χ = –1.3 eV). The fact that the outermost transfer doped ND grain is, most likely, entirely p-type results in an upward shift of the last potential barrier. The vacuum-facing surface of this grain must be covered by a physisorbed acidic water monolayer[36] on its hydrogenated surface[29] forming a rectangular QW with unoccupied molecular orbitals (UMO). In thermodynamic equilibrium, the electrochemical potential of the water adsorbate layer, μ_e^{ads} = –5.2 eV, is aligned with the Fermi level of the outermost diamond grain (Figure 4).

2.6. Double Barrier Resonance Tunneling

Following this model, increasing the applied extracting field will induce band bending along the heterostructure (**Figure 5**) allowing electrons to sequentially tunnel toward the emission sites. The electrons will first gradually fill the lowest allowed electronic levels (subbands) of the last ta-C QW, located before the outermost nanodiamond surface. Then, a resonant tunneling path will eventually open up toward the corresponding UMO in the thin water layer QW (Figure 5a). Once electrons fill all lower unoccupied states in this water layer, alignment with ta-C energy levels will occur. At this moment, electrons are subjected to a double-barrier resonant tunneling (DBRT), due to the overlap of both ta-C QW and water unoccupied states throughout the outermost nanodiamond grain (first barrier) and the vacuum (second barrier) as sketched in Figure 5b. This DBRT will swiftly boost the transmission probability of the electrons, which until now has been almost zero, and give rise to a sudden burst of electrons expressed by an abrupt jump of more than three orders of magnitude in the FE current. This is a current value similar to that which would have been obtained if a gradual turn on FE would have occurred during the increase in the applied field. A further increase of the applied field will lead to the filling of higher sub-band levels in the ta-C QW (Figure 5c), eventually causing further overlaps of ta-C QW and water QW energy levels (Figure 5d) and resulting in additional DBRT toward vacuum. This results in further jumps in the emission current from higher energy states (Figure 5e). Between these jumps no dramatic FE is expected as the supply of electrons is only gradually increased.

The hysteresis during the ramp down of the voltage is caused by the fact that UMO states in the water layer QW are kept charged from the upward field sweep. The electron emission will be sustained as long as the bias voltage will allow electron transport over aligned states of both ta-C and water QWs to favorite DBRT. Decreasing the voltage will both diminish the carriers' supply to the QWs and gradually cancel overlapping states due to energy level shift. Therefore, a gradual decline in the emission current with a slight hump takes place. Then, an abrupt switch off occurs when no replenishment and/or no alignment of energy levels any longer exist, thus promptly impeding DBRT conditions. This mechanism, even though

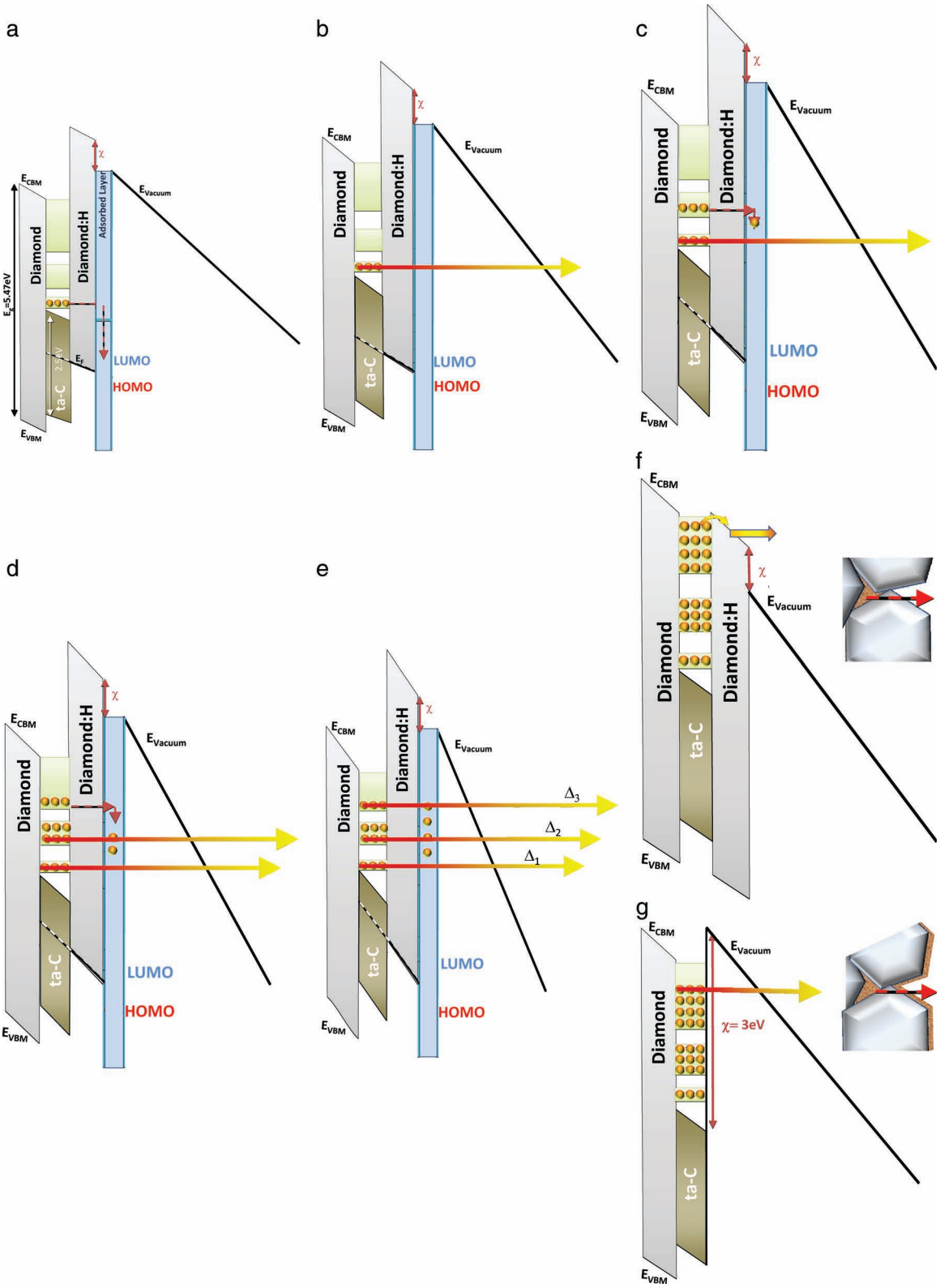

Figure 5. Schematic band bending of the emission site structures following different FE stages as marked on curves in Figure 2 and 3a. a) UNCD:H:H_2O layer during an increasing applied field showing electrons filling from the ta-C QW's electronic levels to the water layer's UMO. b) Alignment between the ta-C and adsorbate QW occurs and gives rise to a double-barrier resonant tunneling yielding the first emission burst of electrons (switch-on). c) Further increase of the field leads to filling of higher subband levels in ta-C QW. d) Further overlaps with the water QW energy levels and another double-barrier resonant tunneling. e) Additional alignment and double-barrier resonant tunneling emission. f) UNCD:H layer under applied field after in situ heating. g) UNCD:H covered by ta-C thin layer under applied field before surface treatment sequences.

streamlined, results in the formation of a memory effect in the current emission for any upward–downward cycle of the applied field.

2.7. Current Emission Plateaus and Effective Barriers Matching

Further confirmation of the above is obtained from the in situ, heating (300 °C) experiments. In this state, transfer doping and water adsorbate is removed resulting in very poor FE with no hysteresis (Figure 2, orange line). The resulting energy band diagram is a symmetric aligned heterostructure of all the nanodiamond potential barriers as represented in Figure 5f. The emission process is now governed by electrons transferring from the ta-C QWs to the conduction band minima of the outermost ND, still benefiting from negative electron affinity , before escaping to vacuum.

The FE between the abrupt jumps was found to be monotonous and to follow the standard FN behavior given by:

$$\ln\left(\frac{J}{E^2}\right) = -6.83 \times 10^7 \frac{\phi^{3/2}}{\beta}\frac{1}{E} + C \qquad (2)$$

A plot of $\ln(J/E^2)$ versus $1/E$ should yield a straight line with a slope, Δ, given by $\Delta = \phi^{3/2}/\beta$, where ϕ is the work function, β is the geometric field enhancement factor, and C is constant. The FN plot of the FE data in the regions between the abrupt jumps is shown in Figure 6. Indeed, they consists of straight lines with ever decreasing slopes (Δ_1, Δ_2, Δ_3). The differences between the respective slopes of each plateau indicate that consecutive current steps are from states with a lower effective barrier i.e., ϕ_1, ϕ_2, ϕ_3, with ϕ_1, ϕ_2, and ϕ_3 corresponding to the first, second, and third current jumps, proving that FE of consecutive steps originate from higher energy levels. Quantitative analysis of the three lines of the FN plot (**Figure 6**), taking for value $\beta = 10$ for all plateaus (as roughly deduced from the UNCD surface smoothness), yields $\phi_1 = 2.8 \pm 0.1$ eV, $\phi_2 = 1.6 \pm 0.4$ eV, and $\phi_3 = 1.2 \pm 0.3$ eV. A rough comparison of these qualitative values agree fairly well with the three energy levels ranges, which yield effective barriers ranges $\phi_1 = 2.6$–2.8 eV, $\phi_2 = 2.0$–2.4 eV, and $\phi_3 = 0.4$–1.9 eV described by the emission mechanism from first, second, and third energy sub-bands in the representative ta-C QWs.

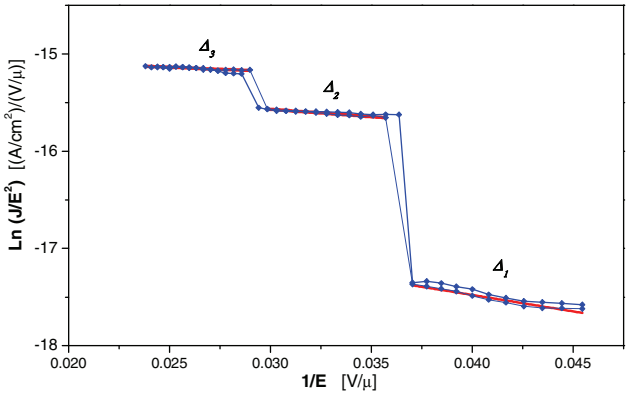

Figure 6. FN plots of FE cycles from UNCD:H:H_2O. Δ_1, Δ_2, and Δ_3 are the slopes corresponding to the first, second, and third current FE plateaus results from Figure 2.

3. Conclusions

A reversible memory switching of the current field emission was experimentally observed for the first time in hydrogen-terminated, humidity-covered ultrananocrystalline diamond layers.

The current emission observations for the sequenced surface treatments of a UNCD layer showed progressive improvement in the switching hysteresis and the in situ heating (evaporation of a water layer from the surface) annulled all current emission phenomena from the sample.

A simplified model relying on characterizations results and physical properties is proposed to explain the peculiar experimental observations. In it, the material is modeled as being composed of a sequence of heterojunctions formed by ta-C QW and ND barriers. The last two heterojunctions (ta-C/ND/adsorbate layer/vacuum) form a double barrier tunneling junction where resonance tunneling occurs when the energy levels of the ta-C QW are aligned with those of the adsorbate layer. The experimental findings described in this paper present a new hysteresis phenomenon in electron field emission that may offer unthinkable applications in carbon-based nanoscale devices.

4. Experimental Section

The samples used were ultrananocrystalline undoped diamond films,[20] about 300 nm thick, grown on quartz by a microwave plasma-enhanced process using an argon rich mixture of Ar/CH_4 at a low temperature of 500 °C. Surface treatment of the samples consisted of a thorough cleaning in acids and exposure to pure hydrogen plasma in a chemical vapor deposition reactor at 650 °C for 40 min followed by exposure to humid air.

FE measurements were performed in an ultrahigh vacuum system (10^{-9} Torr) at room temperature. A spherical anode "tip" (1 mm radius) was mounted on a computer-controlled piezo-driven stage, set at distances 20 to 60 μm from the sample surface. Variable negative voltages (0–5 kV) were applied to the cathode surface relative to the extracting anode. Top silver paint contacts (Ohmic) were used to contact the sample surface with the cathode. The measurements consisted of gradually ramping up the voltage between the cathode and anode, set at fixed distances, while measuring the emission current as function of voltage, i.e., of electric field E. The entire experiment was performed automatically under computer control. Several up/down cycles were performed at the same spot, as well as at different spots, on the sample and for different cathode–anode set distances. Some measurements were performed (at room temperature) on samples following in situ heating to 300 °C.

Acknowledgements

R.K. and M.T. thank the Russell Berrie Nanotechnology Institute for partial financial support.

Received: September 15, 2011
Revised: November 23, 2011
Published online: February 10, 2012

[1] W. Lu, C. M. Lieber, *Nat. Mater.* **2007**, *6*, 841.
[2] J. Ouyang, C. W. Chu, C. R. Szmanda, L. Ma, Y. Yang, *Nat. Mater.* **2004**, *3*, 918.
[3] D. R. Stewart, D. A. A. Ohlberg, P. A. Beck, Y. Chen, S. R. Williams, J. O. Jeppesen, K. A. Nielsen, J. F. Stoddart, *Nano Lett.* **2004**, *4*, 133.
[4] S. Bhattacharyya, S. J. Henley, E. Mendoza, L. Gomez-Rojas, J. Allam, S. R. P. Silva, *Nat. Mater.* **2005**, *5*, 19.
[5] K. B. K. Teo, E. Minoux, L. Hudanski, F. Peauger, J. P. Schnell, L. Gangloff, P. Legagneux, D. Dieumegard, G. A. J. Amaratunga, W. I. Milne, *Nature* **2005**, *437*, 968.
[6] Y. Li, A. Sinitskii, J. M. Tour, *Nat. Mater.* **2008**, *7*, 966.
[7] V. Litovchenko, A. Evtukh, Y. Kryuchenko, N. Goncharuk, O. Yilmazoglu, K. Mutamba, H. L. Hartnagel, D. Pavlidis, *J. Appl. Phys.* **2004**, *96*, 867.
[8] A. V. Karabutov, V. D. Frolov, V. I. Konov, *Diamond Rel. Mater.* **2001**, *10*, 840.
[9] V. Semet, V. T. Binh, J. P. Zhang, J. Yang, M. A. Khan, R. Tsu, *Appl. Phys. Lett.* **2004**, *84*, 1937.
[10] R. Z. Wang, H. Yan, B. Wang, X. W. Zhang, X. Y. Hou, *Appl. Phys. Lett.* **2008**, *92*, 142102.
[11] L. D. Filip, M. Palumbo, J. D. Carey, S. R. P. Silva, *Phys. Rev. B.* **2009**, *79*, 245429.
[12] W. M. Tsang, S. J. Henley, V. Stolojan, S. R. P. Silva, *Appl. Phys. Lett.* **2006**, *89*, 193103.
[13] L. Gan, E. Baskin, C. Saguy, R. Kalish, *Phys. Rev. Lett.* **2006**, *96*, 196808.
[14] T. Yamada, S. Shikata, C. E. Nebel, *J. Appl. Phys.* **2010**, *107*, 013705.
[15] E. W. Plummer, J. W. Gadzuk, R. D. Young, *Solid State Commun.* **1969**, *7*, 487.
[16] C. B. Duke, M. E. Alfereiff, *J. Chem. Phys.* **1967**, *46*, 923.
[17] J. W. Gadzuk, E. W. Plummer, *Rev. Mod. Phys.* **1973**, *45*, 487.
[18] S. M. Lyth, S. R. P. Silva, *Appl. Phys. Lett.* **2009**, *94*, 123102.
[19] J. C. Madaleno, M. K. Singh, E. Titus, G. Cabral, J. Gracio, L. Pereira, *Appl. Phys. Lett.* **2008**, *92*, 23113.
[20] D. M. Gruen, *Rev. Mater. Sci.* **1999**, *29*, 211.
[21] F. Maier, M. Riedel, B. Mantel, J. Ristein, L. Ley, *Phys. Rev. Lett.* **2000**, *85*, 3472.
[22] P. Strobel, M. Riedel, J. Ristein, L. Ley, *Nature.* **2004**, *430*, 439.
[23] V. Chakrapani, J. C. Angus, A. B. Anderson, S. D. Wolter, B. R. Stoner, G. U. Sumanasekera, *Science* **2007**, *318*, 1424.
[24] L. Gan, C. Saguy, R. Kalish, D. L. Tan, B. K. Tay, D. Gruen, P. Bruno, *Diamond Relat. Mater.* **2009**, *18*, 1118.
[25] J. J. Yang, M. D. Pickett, X. Li, D. A.Ohlberg, D. R. Stewart, R. S. Williams. *Nat. Nanotechnol.* **2008**, *3*, 429.
[26] J. G. Park, W. S. Nam, S. H. Seo, Y. G. Kim, Y. H. Oh, G. S. Lee, U. G. Palik, *Nano Lett.* **2009**, *9*, 4,1713.
[27] E. J. Green, J. W. Choi, A. Boukai, Y. Bunimovich, E. Johnston-Halperin, E. DeIonno, Y. Lu, B. A. Sheriff, K. Xu, Y. S. Shin, H. R. Tseng, J. F. Stoddart, J. R. Heath, *Nature* **2007**, *445*, 414.
[28] H.Goronkin, Y. Yang, *Mater. Res. Soc. Bull.* **2004**, *29*, 805.
[29] A. Laikhtman, A. Lafosse, Y. Le Coata, R. Azriaa, A. Hoffman, *Surf. Sci.* **2004**, *551*, 99.
[30] A. Bolker, C. Saguy, M. Tordjman, L. Gan, R. Kalish, *Phys. Rev. B* **2011**, *83*, 155434.
[31] J. Robertson, *Mater. Sci. Eng. R. Rep.* **2002**, *37*, 129.
[32] B. S. Satyanarayana, A. Hart, W. I. Milne, J. Robertson, *Appl. Phys. Lett.* **1997**, *71*, 1430.
[33] M. Yeganeh, P. R. Coxon, A. C. Brieva, V. R. Dhanak, L. Šiller, Y. V. Butenko, *Phys. Rev. B* **2007**, *75*, 155404.
[34] L. D. Landau, E. M. Lifshitz, *Quantum Mechanics Nonrelativistic Theory*, 3rd ed. Pergamon Press, Oxford **1977**, p. 64.
[35] A. C. Ferrari, A. Libassi, B. K. Tanner, V. Stolojan, J. Yuan, L. M. Brown, S. E. Rodil, B. Kleinsorge, J. Robertson, *Phys. Rev. B.* **2000**, *62*, 11089.
[36] J. J. Mareša, P. Hubík, J. Krištofik, J. Ristein, P. Strobel, L. Ley, *Diamond Relat. Mater.* **2008**, *17*, 1356.